Direct-Indirect Character of the Band Gap in Methylammonium Lead Iodide Perovskite

Eline M. Hutter[1], María C. Gélvez-Rueda[1], Anna Osherov[2], Vladimir Bulović[2], Ferdinand C. Grozema[1], Samuel D. Stranks[2,3*], and Tom J. Savenije[1*]

[1]Opto-electronic Materials Section, Department of Chemical Engineering, Delft University of Technology, van der Maasweg 9, 2629 HZ Delft, The Netherlands [2]Research Laboratory of Electronics, Massachusetts Institute of Technology, 77 Massachusetts Avenue, Cambridge, MA 02139, U.S.A [3]Cavendish Laboratory, JJ Thomson Avenue, Cambridge CB3 0HE, United Kingdom

*e-mail: sds65@cam.ac.uk

*e-mail: T.J.Savenije@tudelft.nl

Abstract

Metal halide perovskites such as methylammonium lead iodide ($CH_3NH_3PbI_3$) are generating great excitement due to their outstanding optoelectronic properties, which lend them to application in high efficiency solar cells and light-emission devices. However, there is currently debate over what drives the second order electron-hole recombination in these materials. Here, we propose that the band gap in $CH_3NH_3PbI_3$ has a direct-indirect character. Time-resolved photo-conductance measurements show that generation of free mobile charges is maximized for excitation energies just above the indirect band-gap. Furthermore, we find that second-order electron-hole recombination of photo-excited charges is retarded at lower temperature. These observations are consistent with a slow phonon-assisted recombination pathway via the indirect band-gap. Interestingly, in the low-temperature orthorhombic phase, fast quenching of mobile charges occurs independent of the temperature and photon excitation energy. Our work provides a new framework to understand the optoelectronic properties of metal halide perovskites and analyze spectroscopic data.

Solar cells based on the metal halide perovskite family of materials including $CH_3NH_3PbI_3$ have been rapidly developed in the past few years, reaching record power conversion efficiencies exceeding 22%.[1–3] This unprecedented progress not only makes hybrid perovskites interesting candidates for photovoltaic applications, but also illustrates their fascinating opto-electronic properties. The outstanding photovoltaic performance of $CH_3NH_3PbI_3$ is mainly due to (i) the high absorption coefficient (ii) high yield of free electrons and holes upon photo-excitation and (iii) excellent charge transport properties.[4–7] Although substantial progress has been made in modeling the dynamics of photo-excited charge carriers in $CH_3NH_3PbI_3$,[8,9] we are yet to fully understand what drives the second order electron-hole recombination in this material. Currently, the conventional idea is that $CH_3NH_3PbI_3$ behaves as a direct band gap semiconductor, where the absorption and emission of photons occur via allowed transitions. This is fundamentally different from indirect band gap semiconductors such as silicon in which both absorption and recombination involve not only photons, but also phonons. This results in lower absorption coefficients than in direct semiconductors,[10] but at the same time recombination is much slower.[11]

Recent theoretical calculations of the band structure of $CH_3NH_3PbI_3$ suggest that the conduction band minimum (CBM) is slightly shifted in k-space with respect to the valence band maximum (VBM), making the fundamental band gap indirect.[12–15] Nevertheless, to date, there are no reports of experimental evidence for the presence of an indirect band gap in $CH_3NH_3PbI_3$ or in any other metal halide perovskite. Furthermore, it remains controversial to what extent the temperature and the crystal phase affects the photo-physics in $CH_3NH_3PbI_3$.[16–18]

Finally, most temperature-dependent spectroscopic studies monitor the charge carrier dynamics at relatively high excitation fluences (*i.e.*, in excess of 1 $\mu J/cm^2$), whereas most processes relevant to solar cell operation happen at much lower illumination intensities.

In this work, we use temperature-dependent Time-Resolved Photoluminescence (TRPL) and Microwave Conductance (TRMC) techniques to study the dynamics of optically-excited charge carriers in $CH_3NH_3PbI_3$ at charge densities comparable to AM 1.5 excitation (see Figure 1). Both techniques show that second order electron-hole recombination is a thermally-activated

process for T > 160 K.[7,19] These results are explained by proposing that photo-excited carriers undergo a phonon-assisted recombination pathway. In the orthorhombic phase (T < 160 K), fast quenching of mobile charges is observed. Finally, we find that this behavior is general for solution-processed perovskite films with a planar or meso-structured morphology, independent of the lead precursor used in the fabrication.

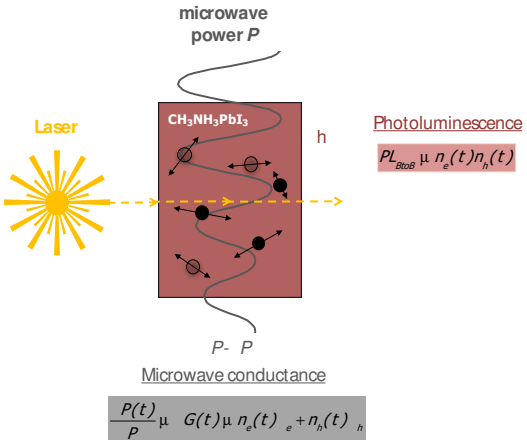

Figure 1: Representation of time-resolved photoluminescence (TRPL) and microwave conductance (TRMC) measurements on a thin film of $CH_3NH_3PbI_3$. In both techniques, electrons (closed circles) are excited to the conduction band by a short laser pulse, leaving mobile holes (open circles) in the valence band. TRMC is used to measure the photo-conductance (ΔG), which scales with the product of the time-dependent concentration and mobility of photo-generated free electrons (μ_e) and holes (μ_h). The sinusoidal line represents the magnitude of the microwave electric field as it passes through the sample. The radiative recombination of these mobile electrons and holes is probed by TRPL, which is a function of the concentrations of electrons ($n_e(t)$) and holes ($n_h(t)$).

Thin (~250 nm), polycrystalline $CH_3NH_3PbI_3$ films were solution-processed on quartz substrates using an acetate-based precursor solution (see Supplementary Figure 1).[20] The TRMC technique was used to measure the photo-conductance ΔG, *i.e.* the difference in conductance of $CH_3NH_3PbI_3$ between dark and after pulsed illumination (see Figure 1). Figures 2a and 2c show ΔG as function of time after excitation of tetragonal (T = 300 K) and orthorhombic (T = 120 K, see also Supplementary Figure 2) $CH_3NH_3PbI_3$, respectively. Directly after photo-excitation (t = 0), ΔG increases due to the formation of free mobile charge carriers. Since no electrodes are attached to the sample, the decrease of the signal over time can only be due to immobilization of charges by trapping or recombination. Hence, these

measurements yield information on the decay processes in $CH_3NH_3PbI_3$ similar to a device under open-circuit conditions. Interestingly, in the tetragonal phase at T = 300 K, the signal observed on excitation at 1.65 eV is significantly higher than at 2.00 eV, while the opposite is true in the orthorhombic phase at T = 120 K.

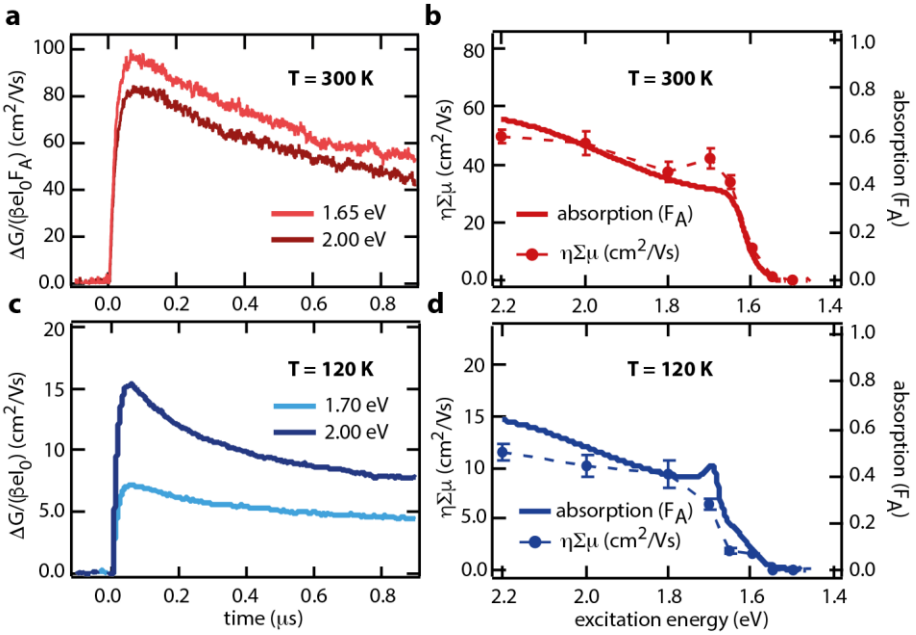

Figure 2. Photo-conductance for a $CH_3NH_3PbI_3$ thin film. Photo-conductance as function of time after excitation at 1.65 eV (λ = 753 nm) and 2.00 eV (λ = 621 nm) for the tetragonal phase at 300 K for an absorbed photon fluence of 8 x 10^8 cm^{-2} per pulse (a). Photo-conductance as function of time after excitation at 1.70 eV (λ = 730 nm) and 2.00 eV (λ = 621 nm) for the orthorhombic phase at 120 K for an incident photon fluence of 2 x 10^{10} cm^{-2} per pulse (c). Comparison of maximum photo-conductance ($\eta\Sigma\mu$, circles) to fraction of absorbed photons at 300 K (b) and 120 K (d), where the absorbed photon fluences are 8 x 10^8 cm^{-2} per pulse for T = 300 K and on the order of 10^9 cm^{-2} per pulse for 120 K. For each excitation wavelength, the photo-conductance was averaged over at least 200 laser pulses and error bars were calculated based on the error in measuring the laser intensity I_0.

The ratio between the number of light-induced free charge carriers and the number of incident photons is defined as the incident yield η. The product of η and the summation of the electron and hole mobilities, $\Sigma\mu$, can be calculated from the maximum value of the photo-conductance ΔG_{max} according to:[21]

$$\eta\sum\mu = \frac{\Delta G_{max}}{I_0 \beta e}$$

Here, I_0 is the number of photons per unit area per pulse, β is the ratio of the inner dimensions of the microwave cell, e the elementary charge.[21] To obtain the quantum yield of free charge carrier generation φ with respect to the number of absorbed (instead of incident) photons, η has to be corrected by the fraction of absorbed photons F_A. Thus, by normalizing $\eta\Sigma\mu$ to F_A, the product of φ and $\Sigma\mu$ is obtained (i.e. $\varphi\Sigma\mu$). If both φ and $\Sigma\mu$ are independent of the excitation wavelength, $\eta\Sigma\mu$ should be proportional to F_A. This can be visualized with a so-called action spectrum, in which the wavelength-dependent $\eta\Sigma\mu$ is directly compared to the F_A spectrum.[22,23] Figures 2b and 2d (dashed lines) show the action spectra for the $CH_3NH_3PbI_3$ thin film at 300 K (b) and at 120 K (d), together with the temperature-dependent F_A spectra (solid lines). Strikingly, for both temperatures the action spectra do not match the F_A spectra. For tetragonal $CH_3NH_3PbI_3$ (Figure 2b), $\eta\Sigma\mu$ reaches a local maximum value at excitation energies close to 1.7 eV (λ = 730 nm). After correction of $\eta\Sigma\mu$ for F_A, see also Figure 2a, $\varphi\Sigma\mu$ at 1.7 eV is close to 100 cm^2/Vs. Considering that the thermal energy at 300 K (26 meV) is much higher than the exciton binding energy of a few milli-electronvolts,[24] most of the excitons will dissociate into free charges and φ is close to unity.[8] Therefore, $\Sigma\mu$ amounts to at least 100 cm^2/Vs for charges excited at 1.7 eV, which is comparable to mobilities reported for single $CH_3NH_3PbI_3$ crystals and thus indicative of the high quality of the polycrystalline films fabricated from the acetate-based precursors.[25] Exciting above 1.8 eV results in $\varphi\Sigma\mu$ values of 80 cm^2/Vs, indicating that φ is approximately 20% lower. Here, we assume that $\Sigma\mu$ is independent of excitation wavelength, which is reasonable in view of the similar decay kinetics (Figure 2a and Supplementary Figure 3). This local maximum in the action spectrum around 1.7 eV is also observed at higher excitation densities, and becomes even more pronounced at lower excitation densities (see Supplementary Figures 4 and 5).

For orthorhombic $CH_3NH_3PbI_3$, in contrast with the tetragonal phase, the $\varphi\Sigma\mu$ values using excitation energies close to 1.7 eV are extremely low (see Figure 2c and Supplementary Figure 6). To understand this, we note that at 120 K, the F_A spectrum is comprised of the band-to-band

continuum and a sharp transition peaking at 1.7 eV that has been attributed to an excitonic feature.[8,26] Hence, we conclude that, for excitation wavelengths that coincide with the excitonic transition (1.7 eV), the generation yield of free charges is much lower than for the band-to-band continuum (≥ 1.8 eV). This implies that in the orthorhombic phase, excitons are less likely to dissociate into free charges than in the tetragonal phase. This observation can be understood from the exciton binding energy being ~16 meV in orthorhombic $CH_3NH_3PbI_3$,[24] which is higher than the thermal energy of 10 meV at 120 K.

To further investigate the generation and recombination pathways of free charges in the different crystal phases, we measured $\varphi\Sigma\mu$ for temperatures ranging from 80 to 340 K using an excitation energy of 2.0 eV, which corresponds to band-to-band excitations in both phases. In the tetragonal (β) phase down to 150 K, $\varphi\Sigma\mu$ is enhanced upon cooling (Figure 3). In contrast, if the temperature is further reduced to 90 K and the crystal structure changes from tetragonal to orthorhombic (γ), $\varphi\Sigma\mu$ decreases substantially.

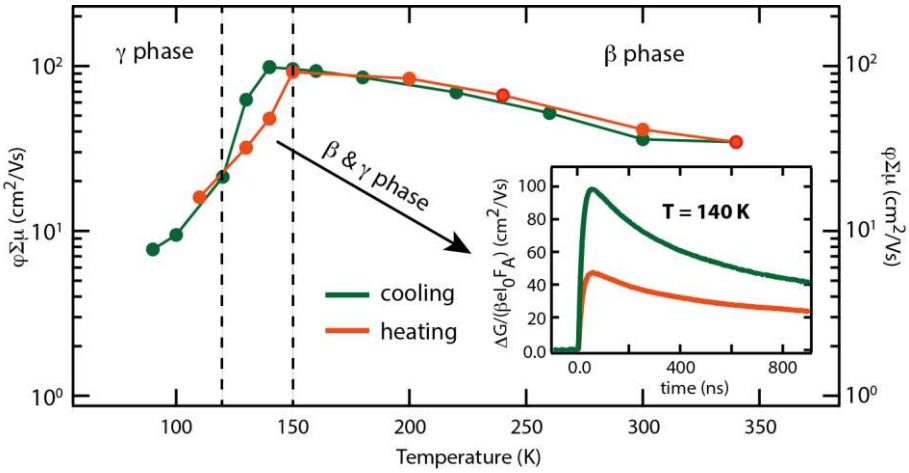

Figure 3. Product of generation yield φ (≤1) and mobility $\Sigma\mu$ as a function of temperature in a $CH_3NH_3PbI_3$ thin film. The film is photo-excited at 2.0 eV (10^{10} absorbed photons/cm^2) and the results are shown for cooling (green) and heating (orange) the film. The time-dependent photo-conductance at 140 K is shown in the inset.

These changes in $\varphi\Sigma\mu$ could be due to a variation of φ and/or $\Sigma\mu$ with temperature. To unravel this, we performed complementary temperature-dependent pulse-radiolysis TRMC experiments, where free electrons and holes are generated by a high-energy electron pulse using

samples prepared in the same way as for the photoconductivity experiments.[27] Similar to the photon-induced TRMC experiments, the initial pulse-induced change in conductivity is determined by the concentration and mobility of the charge carriers. The concentration is tuned by the duration of the accelerator pulse and, therefore, this technique can be used to determine the temperature-dependent mobility.[28] Similar to previous studies,[16,19,28] these measurements confirm that in our $CH_3NH_3PbI_3$ thin films, the mobility increases when the temperature is lowered (Supplementary Figure 7). For these samples $\Sigma\mu$ is proportional to $T^{-1.5}$ down to the phase transition and,[16,19,28] apart from small deviations, no abrupt decrease in the mobility is observed below the phase transition. In other words, the increasing $\varphi\Sigma\mu$ values upon cooling the $CH_3NH_3PbI_3$ thin film down to 150 K are due to an analogous rise in $\Sigma\mu$, whereas the reduced $\varphi\Sigma\mu$ values found for temperatures below 150 K can thus only be attributed to a substantial reduction in φ.

Interestingly, different trends in $\varphi\Sigma\mu$ are found for cooling and heating over the orthorhombic-tetragonal phase transition (see also inset in Figure 3), suggesting the co-existence of tetragonal and orthorhombic phases (see Supplementary Figure 8). For instance, at 140 K (Figure 3), the higher photo-conductance observed upon cooling may be associated with a larger concentration of tetragonal $CH_3NH_3PbI_3$ domains than upon heating. Altogether, these results not only show that the phase transition itself is different for cooling and heating,[29] but also indicate that the low φ is characteristic of the orthorhombic phase. In order to understand the drastic reduction in φ, it is important to note that the exciton binding energy in the orthorhombic phase is only 16 meV.[18,24] According to the Saha equation (Supplementary Figure 9), this results in an exciton population of less than 10% of the photo-excited species for an excitation density of 10^{15} cm^{-3} as used in Figure 3.[6] Although higher values for the exciton binding energy in the orthorhombic phase have been reported,[30] recent temperature-dependent THz spectroscopy studies have confirmed that the majority of excitations results in Drude-like free charges down to 77 K.[16,31] Therefore, given that φ is at least an order of magnitude lower in the orthorhombic phase, this can only to a small extent be attributed to the presence of excitons. Instead, the low value of φ might be due to the occurrence of (sub)-nanosecond decay of mobile electrons and holes, which

is below the temporal resolution of our photon-induced TRMC measurements (see Supplementary Figure 10).

To further investigate the phase-specific recombination pathways, we carried out temperature-dependent TRPL measurements at the maximum emission wavelength (Supplementary Figure 11), which depends both on temperature and the crystal structure, as reported previously.[7,29,32] Figures 4a and 4b show TRPL intensities and TRMC traces for tetragonal $CH_3NH_3PbI_3$ recorded between 260 K and 180 K. Most interestingly, both TRPL and TRMC show the same trends; the lifetime is extended on lowering the temperature.[7,19] Furthermore, at 180 K, both φ and the PL quantum efficiency (PLQE) are close to 1.[7] This means that at this temperature, the radiative recombination (PL) originates primarily from recombination between free mobile electrons and holes. Previously, we have shown that TRPL and TRMC lifetimes in $CH_3NH_3PbI_3$ can be modeled using the same set of kinetic parameters.[33,34] In other words, even at room temperature where the PLQE is typically less than 0.1,[7] second order band-to-band recombination of mobile charges partially leads to PL. The same kinetic model was used to describe the temperature-dependent measurements displayed in Figure 4b (see Supplementary Figure 12). We find that the initial decay is characterized by second order recombination, while recombination between trapped charges and their mobile countercharge dominates at longer timescales (*i.e.* lower concentrations).[33] Figure 4c shows the temperature-dependent mobility and the rate constant k_2, for second order band-to-band electron-hole recombination, obtained from fitting the TRMC traces (see Supplementary Figure 12). Interestingly, the temperature dependence of k_2 indicates that electron-hole recombination is retarded when the temperature is lowered, which we observed to be general for solution-processed perovskite thin films, although we note that the absolute values of k_2 differ for each processing route (see Supplementary Figures 13 to 15). Thus, the second-order band-to-band recombination in tetragonal $CH_3NH_3PbI_3$ is a thermally-activated process under illumination intensities equivalent to 1 sun AM 1.5, implying that there is an energetic barrier for decay.[7,19] This is in contrast with other bulk semiconductors such as GaAs,[35] where recombination becomes faster at lower temperature.

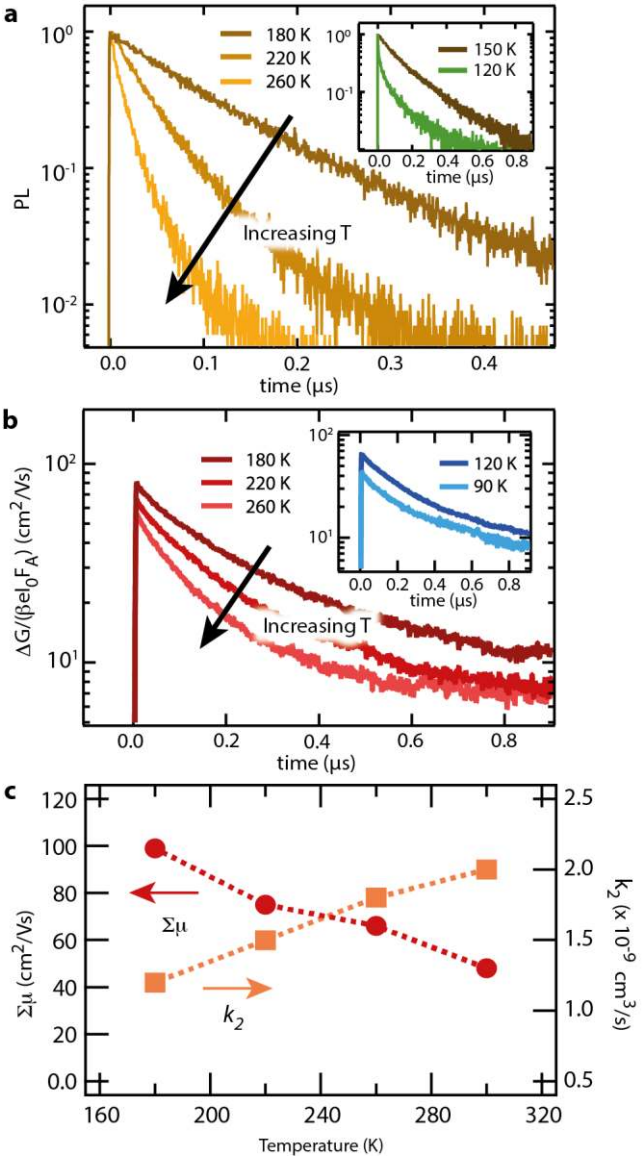

Figure 4. Temperature-dependent PL and TRMC kinetics. a) PL lifetimes recorded at 180 < T < 260 K and 120 K (orthorhombic phase, 742 nm, inset) for $\lambda = 3.0$ eV, $I_0 = 4 \times 10^{12}$ photons/cm^2 per pulse: excitation density of 10^{17} cm^{-3}. b) Temperature-dependent photo-conductance in the tetragonal phase for 180 < T < 260 K and the orthorhombic phase (inset) for $\lambda = 2.0$ eV, $I_0 = 9 \times 10^{10}$ photons/cm^2 per pulse: excitation density of 3×10^{15} cm^{-3}. c) Mobility (circles, left axis) and rate constant k_2 (squares, right axis) for second order electron-hole recombination, obtained from fitting the temperature-dependent TRMC traces as detailed in Supplementary Figure 13.

The inset in Figure 4a shows the PL decay for $CH_3NH_3PbI_3$ at 120 K, for the emission peak centered at 740 nm (see Supplementary Figure 16). The PL decay of the tetragonal phase (T = 150 K) is plotted in the same graph to enable direct comparison, which allows us to visualize that the PL lifetime at 120 K is much shorter than at 150 K. The same trend was observed with

the pulse-radiolysis TRMC experiments, where at least half of the free charges is immobilized within 6 ns (see Supplementary Figure 17). Clearly, the majority of photo-physical products in the orthorhombic phase decay much faster than those in the tetragonal phase. Furthermore, the emission spectra recorded at 90 K and 120 K comprise multiple peaks with different lifetimes (see Supplementary Figure 16), indicating the presence of additional recombination pathways specific for the orthorhombic phase. Additionally, the total integrated intensity of emitted photons at 90 K is lower than at 150 K (see Supplementary Figure 16), which suggests that non-radiative recombination is in competition with radiative events.

Altogether, the above TRPL results show that in the orthorhombic phase, electron-hole recombination occurs on the (sub-)nanosecond timescale, explaining the extremely low yields of mobile charges detected with TRMC.

Discussion

To briefly summarize our results: at 300 K, the generation yield of free charge carriers in $CH_3NH_3PbI_3$ is 20% higher for excitation just above the band-gap (at 1.7 eV) than further above the band gap (> 1.8 eV). Furthermore, in the tetragonal phase, an energetic barrier exists for second-order band-to-band recombination between mobile CB electrons and VB holes. In the orthorhombic phase, both excitons and free charges decay via fast non-radiative recombination pathways, which competes effectively with charge carrier generation.

In order to explain all of these findings, we propose that in the tetragonal phase additional dark states are present, which are located below the optically-accessible conduction band edge. These states are different from shallow traps. That is, if for instance electrons were immobilized in shallow traps, the generation yield of free mobile CB electrons should be enhanced with (i) increasing temperature and (ii) increasing charge carrier concentration. This should lead to a higher $\varphi\Sigma\mu$ with enhanced temperatures (i) and with increasing photon flux (ii). However, as shown in Figure 3 and Supplementary Figures 5, 7 and 15, the opposite trends are observed. Finally, previous TRMC experiments using electron- and hole-selective contacts have shown that both electrons and holes are separately mobile under excitation conditions similar to the

present work.[5,36] Hence, although we do not rule out the presence of shallow trap states, these alone cannot explain the observations reported here. Instead, we propose that these dark states form band-like structures. Excited electrons thermally relax into these bands, yielding highly mobile carriers. Recombination of these electrons back to the ground-state is forbidden, resulting in long charge carrier lifetimes. This model is reminiscent of a semiconductor with an indirect band-gap, where the conduction band minimum (CBM) is shifted in k-space with respect to the valence band maximum (VBM) so that recombination is momentum-forbidden. This explanation is corroborated by theoretical work claiming that the fundamental band gap in $CH_3NH_3PbI_3$ is indirect.[12–15] This has been attributed to collective orientations of the organic cations, which is possible in the tetragonal and cubic crystal phases due to the rotational freedom of the organic cations.[12] However, recent calculations of the band structure of $CH_3NH_3PbI_3$ have shown that Pb spin-orbit coupling results in an indirect band gap, which is therefore also present in systems with random orientations of the organic cation.[15]

To further investigate these indirect transitions and to elucidate whether their origin is related to the Pb spin-orbit coupling[15] or the dipole moment of the organic cation,[12] it will be important both theoretically and experimentally to replace methylammonium with, for example, Cs^+, which does not have a dipole moment. Although there are reports of colloidal systems of Cs-based perovskites[37] and perovskite thin films with low levels of the organic cation substituted with Cs^+,[38] bulk semiconductors based on pure $CsPbI_3$ are not yet of high enough quality in their current form to allow for a fair comparison of their photophysics.[39] It is likely that more stabilized and higher quality embodiments will emerge in the near future to allow for further investigation.

In any case, in both theoretical scenarios, the band diagrams suggest that the CBM is only slightly shifted in k-space, resulting in a manifold of momentum-allowed (direct) transitions for excitation energies close to the absorption onset. Due to the limited density of states (DOS) at the CBM,[15] direct transitions might dominate over indirect transitions at excitation densities higher than used in the present work ($> 10^{17}$ cm^{-3}).[16] To investigate whether direct or momentum-forbidden transitions dominate the absorption onset, rigorous analysis of

absorption spectra, accounting for reflections and excitonic contributions,[40] should be performed.

The direct-indirect nature of the band gap is schematically depicted in Figure 5a. Here, the local minimum in the CB corresponding to a direct transition is denoted by CB_D. We recall here that $\varphi\Sigma\mu$ is larger at 1.7 eV than at 2.0 eV (Figure 2b). We propose that, at an excitation energy of 1.7 eV, thermal relaxation of electrons (direct excitation) into the CBM, which forms an indirect band gap with the VBM, is optimized with respect to relaxation in CB_D. We expect that a fraction of the electrons in CB_D (>1.8 eV) recombines rapidly with VBM holes via direct (radiative) or trap-assisted recombination, resulting in a smaller φ than at 1.7 eV. However, a substantial fraction of electrons excited at >1.8 eV still relaxes into the CBM.

The direct-indirect nature of the band gap in tetragonal $CH_3NH_3PbI_3$ explains why the recombination is enhanced with increasing temperature. This is in contrast with *e.g.* GaAs with a direct band gap,[35] where the second order recombination rate is proportional to $T^{-1.7}$. Recombination via an indirect transition, however, is assisted by phonons. As a consequence, given that there are more phonons when the temperature is raised, indirect recombination is enhanced by increasing the temperature. For direct band gap semiconductors, the second order recombination rate B (T) is proportional to $E_g^2/(k_BT^{3/2})$.[41] To further investigate the thermal activation barrier for second order recombination in $CH_3NH_3PbI_3$, we constructed an Arrhenius plot of the pre-factor ζ (T),[42] which is defined as the ratio between k_2 (T) and B (T). The results are shown in Figure 5b. From the linear slope of ln(ζ (T)) versus reciprocal temperature, an activation energy of 47.0 ± 1.2 meV for second order electron-hole recombination was obtained. Interestingly, this is on the same order of magnitude as the 20 meV[12] to 75 meV[15] difference between the direct and indirect band gaps predicted from theoretical calculations of the band structure. Therefore, thermal energy might assist the release of electrons back into the CB_D where they undergo rapid recombination with holes in the VBM. We note that the low room-temperature PLQE and its enhancement by surface-treatments suggests that at least a fraction of charges decays via non-radiative pathways.[7] The precise influence of shallow or

deep intra-band traps, and their relative competition or synergy with the direct-indirect bandgap character, will be the subject of important future work within the community.

Finally, considering the fast decay of mobile charges in the orthorhombic phase, it is clear that the dominant recombination pathways are different from the tetragonal phase. A plausible scenario for explaining the rapid immobilization of charges is the presence of domains that remain in the tetragonal phase even at low temperature, which could act as efficient recombination centers due to the smaller band gap.[43] A detailed structural study on the phase transition will be published elsewhere. Finally, it is also possible that the orthorhombic lattice does not allow for the formation of an indirect band gap, if the latter is related to orientational freedom of the organic cations.[12]

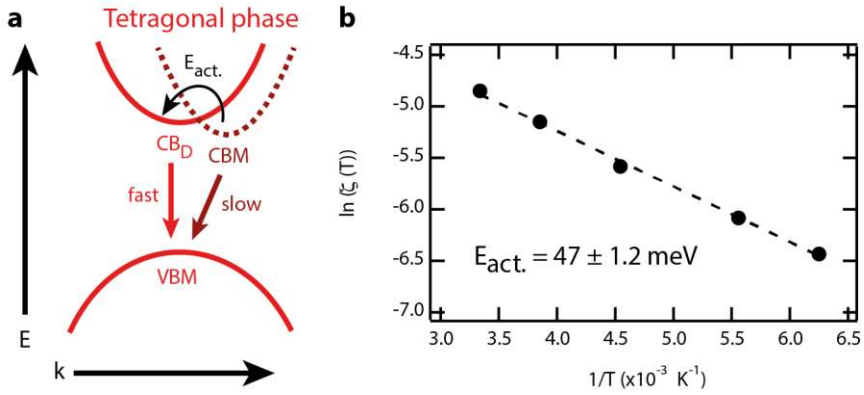

Figure 5. Proposed band diagrams and activation energy for second order recombination in the $CH_3NH_3PbI_3$ thin film. a) Proposed band diagram and for the tetragonal phase. Here, the conduction band minimum (CBM) is slightly shifted in k-space with respect to the valence band maximum (VBM), making the fundamental band gap indirect. The local minimum in the CB corresponding to a direct transition is denoted by CB_D. b) Arrhenius plot of the pre-factor ζ (T),[42] defined as the ratio between the k_2 (T), obtained from fitting the experimental TRMC traces for 160 K < T < 300 K (see Supplementary Figure 12), and the theoretical second order recombination rate B (T).[41] The slope of the linear fit (dotted line) indicates that the activation energy for second order recombination is 47 ± 1.2 meV. Therefore, thermal energy (k_BT) might assist in the release of electrons from CBM to CB_D, which is schematically depicted in (a).

Conclusions

In this work, we used TRMC and PL to investigate the charge carrier dynamics in tetragonal and orthorhombic $CH_3NH_3PbI_3$. Most importantly, we find that in the tetragonal phase, second-

order recombination of mobile electrons and holes occurs via a non-allowed transition, reminiscent of a semiconductor with an indirect band gap. An activation energy of 47.0 ± 1.2 meV was found, which is on the same order of magnitude as the difference between the direct and indirect band gaps predicted from theoretical calculations of the band structure. Additionally, we find that the photo-conductance, reaches maximum values upon excitation at 1.7 eV. This is attributed to direct excitation from the VB into the CBM, which forms an indirect band gap with the VBM. This model also explains why second-order recombination is enhanced with temperature, which is in contrast with other bulk semiconductors such as GaAs.[35]. These effects are not observed in the orthorhombic phase of $CH_3NH_3PbI_3$, in which the major part of the carriers decays rapidly. These insights provide a new framework to understand the optoelectronic properties of metal halide perovskites, rationalize their unique suitability for low-cost photovoltaic and light-emitting devices, and analyze spectroscopic data.

References

1. Stranks, S. D. *et al.* Electron-hole diffusion lengths exceeding 1 micrometer in an organometal trihalide perovskite absorber. *Science* **342,** 341–344 (2013).
2. Yi, C., Li, X., Luo, J., Zakeeruddin, S. M. & Grätzel, M. Perovskite Photovoltaics with Outstanding Performance Produced by Chemical Conversion of Bilayer Mesostructured Lead Halide/TiO2 Films. *Adv. Mater.* **28,** 2964–2970 (2016).
3. http://www.nrel.gov.
4. Wehrenfennig, C., Liu, M., Snaith, H. J., Johnston, M. B. & Herz, L. M. Charge-Carrier Dynamics in Vapour-Deposited Films of the Organolead Halide Perovskite CH3NH3PbI3−xClx. *Energy Environ. Sci.* **7,** 2269–2275 (2014).
5. Ponseca, C. S. *et al.* Organometal halide perovskite solar cell materials rationalized: ultrafast charge generation, high and microsecond-long balanced mobilities, and slow recombination. *J. Am. Chem. Soc.* **136,** 5189–5192 (2014).
6. Johnston, M. B. & Herz, L. M. Hybrid Perovskites for Photovoltaics: Charge-Carrier Recombination, Diffusion, and Radiative Efficiencies. *Acc. Chem. Res.* **49,** 146–154 (2016).
7. Stranks, S. D. *et al.* Recombination Kinetics in Organic-Inorganic Perovskites: Excitons, Free Charge, and Subgap States. *Phys. Rev. Appl.* **2,** 034007 (2014).
8. D'Innocenzo, V. *et al.* Excitons versus free charges in organo-lead tri-halide perovskites. *Nat. Commun.* **5,** 3586 (2014).
9. Brenner, T. M., Egger, D. A., Kronik, L., Hodes, G. & Cahen, D. Hybrid organic-inorganic perovskites: low-cost semiconductors with intriguing charge-transport properties. *Nat. Rev. Mater.* **1,** 15007 (2016).
10. Green, M. A., Ho-Baillie, A. & Snaith, H. J. The emergence of perovskite solar cells. *Nat. Photonics* **8,** 506–514 (2014).
11. Grundmann, M. *The Physics of Semiconductors: An Introduction Including Devices and Nanophysics*. *Springer* (2006).
12. Motta, C. *et al.* Revealing the role of organic cations in hybrid halide perovskite

CH3NH3PbI3. *Nat. Commun.* **6,** 7026 (2015).
13. Zheng, F., Tan, L. Z., Liu, S. & Rappe, A. M. Rashba spin-orbit coupling enhanced carrier lifetime in CH3NH3PbI3. *Nano Lett.* **15,** 7794–7800 (2015).
14. Etienne, T., Mosconi, E. & De Angelis, F. Dynamical Origin of the Rashba Effect in Organohalide Lead Perovskites: A Key to Suppressed Carrier Recombination in Perovskite Solar Cells? *J. Phys. Chem. Lett.* **7,** 1638–1645 (2016).
15. Azarhoosh, P., Frost, J. M., McKechnie, S., Walsh, A. & van Schilfgaarde, M. Relativistic origin of slow electron-hole recombination in hybrid halide perovskite solar cells. *APL Mater.* **4,** 091501 (2016).
16. Milot, R. L., Eperon, G. E., Snaith, H. J., Johnston, M. B. & Herz, L. M. Temperature-Dependent Charge-Carrier Dynamics in CH3NH3PbI3 Perovskite Thin Films. *Adv. Funct. Mater.* **25,** 6218–6227 (2015).
17. Wang, H., Whittaker-Brooks, L. & Fleming, G. R. Exciton and Free Charge Dynamics of Methylammonium Lead Iodide Perovskites Are Different in the Tetragonal and Orthorhombic Phases. *J. Phys. Chem. C* **119,** 19590–19595 (2015).
18. Even, J., Pedesseau, L., Jancu, J.-M. & Katan, C. Importance of Spin–Orbit Coupling in Hybrid Organic/Inorganic Perovskites for Photovoltaic Applications. *J. Phys. Chem. Lett.* **4,** 2999–3005 (2013).
19. Savenije, T. J. *et al.* Thermally Activated Exciton Dissociation and Recombination Control the Carrier Dynamics in Organometal Halide Perovskite. *J. Phys. Chem. Lett.* **5,** 2189–2194 (2014).
20. Zhang, W. *et al.* Ultrasmooth organic-inorganic perovskite thin-film formation and crystallization for Efficient Planar Heterojunction Solar Cells. *Nat. Commun.* **6:6142,** (2015).
21. Savenije, T. J., Ferguson, A. J., Kopidakis, N. & Rumbles, G. Revealing the dynamics of charge carriers in polymer:fullerene blends using photoinduced time-resolved microwave conductivity. *J. Phys. Chem. C* **117,** 24085–24103 (2013).
22. Park, J., Reid, O. G., Blackburn, J. L. & Rumbles, G. Photoinduced spontaneous free-carrier generation in semiconducting single-walled carbon nanotubes. *Nat. Commun.* **6,** 8809 (2015).
23. Kroeze, J. E., Savenije, T. J., Vermeulen, M. J. W. & Warman, J. M. Contactless Determination of the Photoconductivity Action Spectrum, Exciton Diffusion Length, and Charge Separation Efficiency in Polythiophene-Sensitized TiO2 Bilayers. *J. Phys. Chem. B* **107,** 7696–7705 (2003).
24. Miyata, A. *et al.* Direct measurement of the exciton binding energy and effective masses for charge carriers in organic-inorganic tri-halide perovskites. *Nat. Phys.* **11,** 582–587 (2015).
25. Dong, Q. *et al.* Electron-hole diffusion lengths > 175 μm in solution-grown CH3NH3PbI3 single crystals. *Science* **347,** 967–970 (2015).
26. Saba, M. *et al.* Correlated electron–hole plasma in organometal perovskites. *Nat. Commun.* **5:5049,** (2014).
27. Grozema, F. C. & Siebbeles, L. D. A. Charge mobilities in conjugated polymers measured by pulse radiolysis time-resolved microwave conductivity: From single chains to solids. *J. Phys. Chem. Lett.* **2,** 2951–2958 (2011).
28. Gélvez-Rueda, M. C. *et al.* Effect of Cation Rotation on Charge Dynamics in Hybrid Lead Halide Perovskites. *J. Phys. Chem. C* **120,** 16577–16585 (2016).
29. Wehrenfennig, C., Liu, M., Snaith, H. J., Johnston, M. B. & Herz, L. M. Charge carrier recombination channels in the low-temperature phase of organic-inorganic lead halide perovskite thin films. *APL Mater.* **2,** 081513 (2014).
30. Fang, H. H. *et al.* Photophysics of organic-inorganic hybrid lead iodide perovskite single crystals. *Adv. Funct. Mater.* **25,** 2378–2385 (2015).
31. Karakus, M. *et al.* Phonon-Electron Scattering Limits Free Charge Mobility in Methylammonium Lead Iodide Perovskites. *J. Phys. Chem. Lett.* **6,** 4991–4996 (2015).
32. Wu, K. *et al.* Temperature-dependent excitonic photoluminescence of hybrid organometal halide perovskite films. *Phys. Chem. Chem. Phys.* **16,** 22476–22481

(2014).
33. Hutter, E. M., Eperon, G. E., Stranks, S. D. & Savenije, T. J. Charge Carriers in Planar and Meso-Structured Organic-Inorganic Perovskites: Mobilities, Lifetimes and Concentrations of Trap States. *J. Phys. Chem. Lett.* **6,** 3082–3090 (2015).
34. Bi, Y. *et al.* Charge Carrier Lifetimes Exceeding 15 Microseconds in Methylammonium Lead Iodide Single Crystals. *J. Phys. Chem. Lett.* **7,** 923–928 (2016).
35. 't Hooft, G. W. & van Opdorp, C. Temperature dependence of interface recombination and radiative recombination in (Al, Ga)As heterostructures. *Appl. Phys. Lett.* **42,** 813–815 (1983).
36. Ponseca, C. S. *et al.* Mechanism of Charge Transfer and Recombination Dynamics in Organo Metal Halide Perovskites and Organic Electrodes, PCBM and Spiro-OMeTAD: Role of Dark Carriers. *J. Am. Chem. Soc.* **137,** 16043–16048 (2015).
37. Protesescu, L. *et al.* Nanocrystals of Cesium Lead Halide Perovskites (CsPbX3, X = Cl, Br, and I): Novel Optoelectronic Materials Showing Bright Emission with Wide Color Gamut. *Nano Lett.* **15,** 3692–3696 (2015).
38. Saliba, M. *et al.* Cesium-containing Triple Cation Perovskite Solar Cells: Improved Stability, Reproducibility and High Efficiency. *Energy Environ. Sci.* **9,** 1989 (2016).
39. Eperon, G. E. *et al.* Inorganic caesium lead iodide perovskite solar cells. *J. Mater. Chem. A* **3,** 19688–19695 (2015).
40. Saba, M., Quochi, F., Mura, A. & Bongiovanni, G. Excited State Properties of Hybrid Perovskites. *Acc. Chem. Res.* **49,** 166–173 (2016).
41. Gfroerer, T. H., Priestley, L. P., Weindruch, F. E. & Wanlass, M. W. Defect-related density of states in low-band gap In x Ga 1-x As / In As y P 1-y double heterostructures grown on InP substrates. *J. Appl. Phys.* **94,** 1738–1743 (2003).
42. Ferguson, A. J., Kopidakis, N., Shaheen, S. E. & Rumbles, G. Dark carriers, trapping, and activation control of carrier recombination in Neat P3HT and P3HT:PCBM blends. *J. Phys. Chem. C* **115,** 23134–23148 (2011).
43. Kong, W. *et al.* Characterization of an abnormal photoluminescence behavior upon crystal-phase transition of perovskite CH3NH3PbI3. *Phys. Chem. Chem. Phys.* **17,** 16405–11 (2015).

Film preparation

Glass substrates were washed sequentially with soap, de-ionized water, isopropanol, acetone and finally treated under oxygen plasma for 10 minutes. Thin films of $CH_3NH_3PbI_3$ were solution-processed by employing a methylammonium iodide (CH_3NH_3I) and lead acetate Pb(Ac)2·3H2O precursor mixture. CH_3NH_3I (Dyesol) and $Pb(Ac)_2·3H_2O$ (Sigma-Aldrich) were dissolved in anhydrous *N*,*N*-dimethylformamide at a 3:1 molar ratio with final concentration of 37 wt%. The precursor solution was spin-coated at 2000 rpm for 45 seconds in a nitrogen-filled glovebox, and the substrates were then dried at room temperature for 10 minutes before annealing at 100°C for 5 minutes. For the meso-structured samples, mesoporous alumina layers of ~400 nm were formed by spin-coating a solution of ~20 nm alumina nanoparticles in propan-2-ol on glass and drying at 150 °C. A diluted version (30 wt%) of the

same acetate precursor solution was then spin-coated onto the mesoporous film at 2000 rpm for 45 seconds in a nitrogen-filled glovebox and the film dried at room temperature for 10 minutes before annealing at 100°C for 5 minutes. For the PbI_2-based samples, the 'dripping' technique was employed. Here, an equimolar (0.75 M, total 45 wt%) solution of CH_3NH_3I (Dyesol) and PbI_2 (Alfa Aesar) was prepared in DMF and spin-cast at 5000 rpm for 35 s. After 6 s, 150 μL chlorobenzene was deposited on the spinning sample in order to induce rapid crystallization. After spinning, the samples were immediately heated at 100 °C for 10 minutes. All samples were then stored in a nitrogen-filled glovebox until used.

X-Ray Diffraction

X-Ray Diffractograms were collected from $CH_3NH_3PbI_3$ thin films on boron-doped Si(100) substrates using PANalytical X'Pert Pro Multi-Purpose Diffractometer operated at 40 kV and 40 mA (Cu K-alpha radiation- 1.5418 Å) in Bragg-Brentango geometry. An Oxford Cryosystems PheniX Cryostat was employed for low temperature measurements. Data analysis was carried out using the Panalytical X'pert Highscore Plus program and corrections for stage and substrate thermal expansion were made.

Optical Characterization

Absorption and transmission spectra were recorded with a Perkin-Elmer Lambda 1050 spectrophotometer equipped with an integrated sphere. The thin films were placed in front of the sphere to measure the fraction of transmitted light (F_T) and under an angle of 10° inside the sphere to detect the total fraction of reflected and transmitted photons (F_{R+T}). From here, we calculated the fraction of absorbed light (F_A):

$$F_A = 1 - F_{T+R} \quad (1)$$

The fraction of reflected light (F_R) was determined from:

$$F_R = 1 - F_A - F_T \quad (2)$$

The absorption coefficient α is often calculated from the transmission spectrum using:

$$\frac{I_L}{I_0} = e^{-\alpha L} \quad (3)$$

Where I_L/I_0 equals F_T for a sample of thickness L with negligible reflection. However, since $CH_3NH_3PbI_3$ films are highly reflective, α was obtained from:

$$\frac{F_T}{1-F_R} = e^{-\alpha L} \quad (4)$$

The low-temperature transmission spectrum was measured under nitrogen using a Cary 500i UV-Vis-NIR Dual-Beam Spectrophotometer with a liquid-nitrogen-cooled Linkum Scientific FTIR 600 Freezing stage for temperature control. F_A was calculated from (2), thereby neglecting possible temperature dependence of F_R. For the temperature-dependent TRPL measurements the samples were placed in a nitrogen-filled cryostat. The PL emission spectra and PL lifetimes at the maximum emission wavelength were recorded using an Edinburgh LifeSpec spectrometer equipped with a single photon counter. The $CH_3NH_3PbI_3$ films were excited at 405 nm with a picosecond pulsed diode laser (Hamamatsu, M8903-01, $I_0 = 4 \times 10^{12}$ photons/cm^2, repetition rate 0.1 MHz).

Photo-conductance measurements

The $CH_3NH_3PbI_3$ films on quartz substrates were placed in a sealed resonance cavity inside a nitrogen-filled glovebox. The photon-induced Time Resolved Microwave Conductivity (TRMC) technique was used to measure the change in microwave (8-9 GHz) power after pulsed excitation (repetition rate 10 Hz).[21] The excitation wavelength of the LASER was varied from 518 nm (2.4 eV) to 828 nm (1.5 eV); the incident photon flux was adjusted by using different

filters. For each excitation wavelength, the photo-conductance was averaged over at least 200 laser pulses. The laser intensity, I_0, was determined using a Coherent power meter with an adjustable detection range. The inaccuracy of determination of I_0 due to fluctuations of the laser is approximately ± 0.1 mJ, which is taken into account in the error analysis of the data. The illuminated sample area is ~2.5 cm^2. The time-resolved change in conductance ΔG(t) was obtained from the photo-excitation-induced change in microwave power ΔP(t), which are related by a sensitivity factor K:

$$\frac{\Delta P(t)}{P} = -K\Delta G(t) \quad (5)$$

The rise of ΔG is limited by the width of the laser pulse (3.5 ns FWHM) and the response time of our microwave system (18 ns). The slow repetition rate of the laser of 10 Hz ensures full relaxation of all photo-induced charges to the ground state before the next laser pulse hits the sample. A detailed description of this technique can be found in Ref. [21].

Pulse-radiolysis TRMC measurements

Four substrates each covered with ~75 cm^2 $CH_3NH_3PbI_3$ (thickness ~ 250 nm) were used to scratch off 35 mg of material, which was placed in a polyether ether ketone (PEEK) holder. To protect the $CH_3NH_3PbI_3$ from moisture and air, it was covered with poly-methyl-methacrylate (PMMA), drop-casted from a 10 mg/mL PMMA/chlorobenzene solution. Pulse-radiolysis TRMC (PR-TRMC) measurements involve the generation of charge carriers through irradiation by a short pulse of high-energy electrons (3 MeV) and the monitoring of the changes in conductivity due to mobile charge carriers using high frequency microwaves (28-38 GHz).[27,44] The conductivity transients shown were obtained at 32 GHz. Similar to the photon-induced TRMC, the change of conductivity is proportional to the absorbed microwave power:

$$\frac{\Delta P}{P} = A\Delta\sigma \quad (6)$$

The experimental frequency dependence of *ΔP/P* can be fitted with an analytical expression to determine the dielectric constant, ε, and change in conductivity, $\Delta\sigma$.[44]

The mobility is then calculated by:

$$\Delta\sigma = e \sum N_p(0)\, \mu \quad (9)$$

Where $N_p(0)$ is the initial concentration of charge carriers at the end of the pulse and μ the sum of the mobilities for electrons and holes. $N_p(0)$ is a function of the mass of material (m), volume of the sample holder (V_{sh}), irradiation energy deposited in the sample (D) and of the radiation-ionization energy required for the generation of an electron-hole pair (E_p):

$$N_p(0) = \frac{D}{E_p * 1.6 * 10^{-19} \frac{J}{eV}} \frac{m}{V_{sh}} \quad (7)$$

D is proportional to the electron density of the material and for perovskites has been determined to be ~1 J/Kg/nC.[28] The latter is derived from previous radiation dosimetry experiments. E_p has been determined according to Klein's theoretical model[45] and Alig's equation[46] for semiconductor materials, which relates it to the band gap of the material, phonon losses and the residual kinetic energy:

$$E_p = 2.73\, E_g + 0.55\ [eV] \quad (8)$$

In the PR-TRMC set up, the cell is contained in a cryostat in which the temperature can be varied between -150°C and 200°C. The temperature was maintained for ~15 min before doing the actual measurement in order to assure the equilibrium of the system. The overall time response of the set-up is limited by the rise time of the detector diode and the length of the excitation pulse (~1 ns). The frequency scans (28-38 GHz) were measured at a pulse length of 200 ps, corresponding to an initial charge carrier concentration of 4.7×10^{14} cm^{-3}.

44. Warman, J. M. *et al.* Charge Mobilities in Organic Semiconducting Materials Determined by Pulse-Radiolysis Time-Resolved Microwave Conductivity: π-Bond-

Conjugated Polymers versus π–π-Stacked Discotics. *Chem. Mater.* **16,** 4600–4609 (2004).
45. Klein, C. A. Bandgap Dependence and Related Features of Radiation Ionization Energies in Semiconductors. *J. Appl. Phys.* **39,** 2029–2038 (1968).
46. Alig, R. C. & Bloom, S. Electron-hole-pair creation energies in semiconductors. *Phys. Rev. Lett.* **35,** 1522–1525 (1975).

Acknowledgments

This work was supported by the Netherlands Organization for Scientific Research (NWO) under the Echo grant number: 712.014.007. S.D.S. has received funding from the People Programme (Marie Curie Actions) of the European Union's Seventh Framework Programme (FP7/2007-2013) under REA grant agreement number PIOF-GA-2013-622630. The authors thank Arjan Houtepen, Alexander Achtstein and Dane deQuilettes for fruitful discussions. Wiel Evers is acknowledged for technical assistance.

Author contributions

E.M.H. performed and analyzed the photon-induced TRMC, optical absorption and (TR)PL measurements under the supervision of T.J.S. S.D.S. prepared the samples and performed additional optical absorption measurements. A.O. performed XRD and SEM measurements and M.C.G.-R. and F.C.G. performed pulse-radiolysis TRMC measurements. E.M.H. and T.J.S. conceived the idea and wrote the manuscript together with S.D.S.

Additional Information

Supplementary information is available in the online version of the paper. Reprints and permissions information is available online at www.nature.com/reprints. Correspondence should be addressed to S.D.S. or T.J.S.

Competing financial interests

The authors declare no competing financial interests.